c(4 × 2) and related structural units on the $SrTiO_3$(001) surface: Scanning tunneling microscopy, density functional theory, and atomic structure

A. E. Becerra-Toledo,[1,a)] M. S. J. Marshall,[2,b)] M. R. Castell,[2] and L. D. Marks[1]
[1]*Department of Materials Science and Engineering, Northwestern University, Evanston, Illinois 60208, USA*
[2]*Department of Materials, University of Oxford, Parks Road, Oxford OX1 3PH, United Kingdom*

(Received 25 January 2012; accepted 3 May 2012; published online 4 June 2012)

Density functional theory is used to simulate high-bias, constant-current scanning tunneling micrographs for direct comparison with experimental images. Coupled to previous spectroscopic data, these simulations are used to determine the atomic structure of Ti-rich nanostructures on strontium titanate (001) surfaces. These nanostructures have three consecutive TiO_x surface layers and exploit the distinctive structural motif of the c(4 × 2) reconstruction as their main building block. A structural model of a characteristic triline defect is also proposed. © *2012 American Institute of Physics*. [http://dx.doi.org/10.1063/1.4719212]

I. INTRODUCTION

Strontium titanate ($SrTiO_3$) has been regarded as the archetypal model system for the perovskite class of solid oxides and has garnered much attention for possible use in technological applications including photocatalysis,[1] thin film growth of superconducting cuprates,[2] and novel oxide heterostructures which exploit, for example, the formation of a two-dimensional electron gas at interfaces with $LaAlO_3$.[3] Its performance in most such applications crucially depends on its surface structure and composition. This has motivated a large number of surface studies on $SrTiO_3$, mostly regarding its dominant (001) orientation.[4–14]

The c(4 × 2) $SrTiO_3$(001) surface reconstruction was structurally solved by Erdman *et al.*[9] using a combination of transmission electron diffraction, direct methods, and density functional theory (DFT). Like other $SrTiO_3$(001) reconstructions,[8,11,13,15] the c(4 × 2) was found to have a double-layer TiO_2 termination, with the second topmost layer qualitatively resembling the arrangement of TiO_2 planes in bulk $SrTiO_3$. The top layer consists of a periodic pattern based on a main feature, which in turn consists of a clustered quartet of edge-sharing TiO_5 polyhedra.

In the particular case of the c(4 × 2) reconstruction, it is well known that the quartets (which are roughly squares of c(2 × 2) dimensions) run in corner-sharing alignment along only one [001]-type direction, with each row of quartets "out of phase" with the next row. The structure is shown in its polyhedral representation in Figs. 1(a) and 1(b).

The generation of a novel type of Ti-rich linear surface nanostructures on $SrTiO_3$(001) surfaces, the so-called nanolines, has been reported upon sputtering and ultra-high vacuum (UHV) annealing;[4] the dominant nanolines are the dilines and trilines. These show potential for use as templates for nanoscale patterning of molecules or nanoparticles.[16,17] The present paper reports on the use of high-bias scanning tunneling micrograph simulations based on DFT computations, in an attempt to determine atomic-level structural solutions for the dilines and trilines. It is determined that the aforementioned polyhedral motif is also an important building block in these nanostructures.

II. METHODS

A. Experimental

Single-crystalline, 0.5 wt. % Nb-doped $SrTiO_3$(001) wafers (7 × 2 × 0.5 mm) were commercially purchased (PI-KEM Ltd, United Kingdom) for scanning tunneling microscopy (STM) studies in an ultra-high vacuum JEOL JSTM4500S. Electron doping with Nb was necessary to render the specimens electrically conductive for experimental analysis.

c(4 × 2)-reconstructed surfaces were produced in the following manner: the specimens were etched for 10 min with a buffered NH_4-HF solution, shown by Kawasaki *et al.*[12] to preferentially remove surface SrO; Ar^+-sputtering inside the UHV chamber (base pressure 10^{-8} Pa) was carried out with a VG Microtech gun for 10 min with 0.5 kV ion energy and a 45° incidence angle; finally, UHV resistive heating for 15 min at 1200 °C was performed by applying a direct current through the samples.[4] Nanostructured surfaces were obtained via Ar^+-sputtering for 10 min with 1.0 kV ion energy and a 45° incidence angle, followed by a 2 hr UHV anneal at 900 °C.

B. Density functional theory

First-principle density functional calculations were performed to model the different surfaces, using the repeated slab configuration. All DFT calculations were carried out using an augmented plane wave + local orbital basis set with the full-electron-potential WIEN2k code.[18] Every structure modeled was relaxed until the residual force on each atom was below 0.2 eV/Å; tests verified that this force tolerance was sufficient to establish the atomic positions within the

a)Author to whom correspondence should be addressed. Electronic mail: andres@u.northwestern.edu.
b)Present address: Department of Applied Physics, Yale University, New Haven, Connecticut 06510, USA.

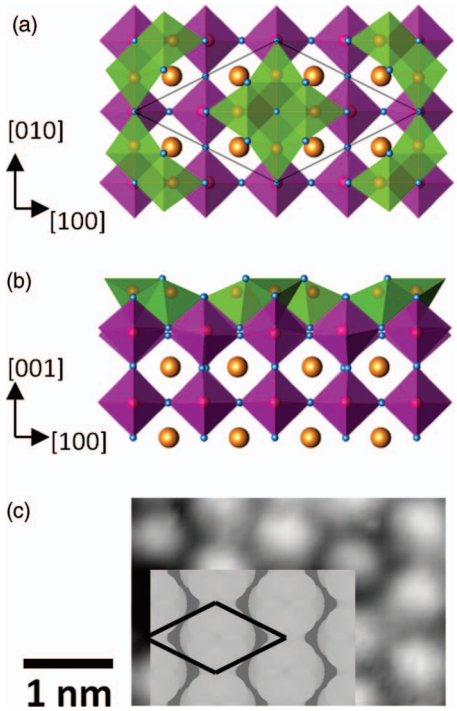

FIG. 1. Polyhedral representation of the c(4 × 2) reconstructed surface in (a) plan view, with the unit cell outlined, and in (b) profile view. All such figures show Sr in orange, Ti in red, and O in blue. Ti-centered polyhedra are colored as follows: purple for 6-fold, green for 5-fold, and black for 4-fold coordination. (c) DFT-based 2.0 V STM image simulation, superposed to experimental image (2.0 V bias, 0.1 nA current).

experimentally available positional uncertainty. The exchange-correlation functional of choice was the Perdew-Burke-Ernzerhof (PBE, Ref. 19) implementation of the generalized gradient approximation. This functional is known to overestimate the cation *d* – anion *sp* hybridization in strongly correlated systems, so other functionals (PBE0, PBE+U, MBJLDA) were tested with preliminary structural models; despite the increased computational expense, no discernible difference was ultimately found in the STM simulations within the available spatial resolution.

The c(4 × 2) slab consisted of 13 atomic layers, with the following alternation of planes: TiO_2 – TiO_2 – SrO – TiO_2 – SrO – TiO_2 – SrO – TiO_2 – SrO – TiO_2 – SrO – TiO_2. Meanwhile, the nanoline models varied in thickness, with the final slabs consisting of 11 atomic layers. Muffin-tin radii of 2.40 (Sr), 1.68 (Ti), and 1.50 (O) bohrs were consistently employed, along with a maximum *K* value of 5.25/1.5 bohrs^{-1} for the plane wave expansion. In each model, a *k*-point mesh equivalent to a 8 × 8 × 8 mesh for a bulk $SrTiO_3$ unit cell was used. A vacuum spacing of at least 10 Å between slabs was used. The optimized lattice parameter value of $a^{\mathrm{PBE}}_{\mathrm{SrTiO_3}} = 3.944$ Å was enforced in the dimensions parallel to the surface plane.

While these parameters are adequate for STM image simulations, accurate total energy calculations would require much thicker slabs, as well as functionals better suited for strongly correlated systems, as discussed above. Furthermore, given the stoichiometry differences between the numerous models, no thermodynamic analysis or prediction is possible without assuming values for the relevant chemical potentials (in this case, TiO_2 and O_2). Since these variables were not experimentally well controlled, total energy considerations are by and large excluded from the present analysis.

C. Scanning tunneling micrograph simulations

The STM image simulations build on the work of Tersoff and Hamann,[20] who utilized Bardeen's tunneling theory.[21] The latter treats the tip-sample system as a metal-insulator-metal junction, uses the independent wavefunctions on either side of the tunneling barrier and approximates them as being roughly orthogonal. The limit of low temperature and sample-tip bias, coupled to the simplification of the tip to *s*-type states, leads to the well-known Tersoff-Hamann approximation, whereby the tunneling current I_t is proportional to the local density of states around the Fermi energy of the specimen, E_F,

$$I_t \propto \rho(\boldsymbol{r}, E_F) \equiv \sum_{\mu} |\psi_\mu(\boldsymbol{r})|^2 \delta(\varepsilon_\mu - E_F), \tag{1}$$

where ψ_μ is the sample wavefunction with eigenvalue ε_μ. This result opened up the door to first-principle methods such as DFT; however, this relation breaks down for bias voltages larger than 100 mV, as is the case with doped $SrTiO_3$, which requires biases of larger than 1 V.[22]

Stokbro *et al.*[23] attempted to extend Tersoff-Hamann theory not only to the high-bias regime but also to include non-spherical tip states. Their derivation was followed herein, except that the tip wavefunction expansion used by Chen[24] was employed instead; otherwise, low-energy surface states are incorrectly weighted more heavily, even though elastic tunneling to high-energy states is more probable due to the smaller effective tunneling barrier. In this case, and ignoring higher-order angular tip states for the present study, we arrive at a modified relation, for a bias voltage V_b

$$I_t \propto \int_{E_F}^{E_F + e \cdot V_b} \kappa(\varepsilon)^{-2} \rho(\boldsymbol{r}, \varepsilon) d\varepsilon, \tag{2}$$

where

$$\kappa(\varepsilon) = \hbar^{-1} \sqrt{2 m_e (\varphi_t + E_F + e \cdot V_b - \varepsilon)} \tag{3}$$

is the inverse decay length of the electron states in vacuum for energy ε, φ_t is the tip workfunction, m_e is the mass of an electron, and *e* is its charge.

In terms of the implementation via DFT, this implies that after full relaxation and convergence of a structure, the unoccupied states between E_F and $E_F + eV_b$ must be artificially populated but with the regular population multiplied by a weighting factor proportional to $\kappa(\varepsilon)^{-2}$. One question is what E_F value to use. In the bulk Nb-doped $SrTiO_3$ crystal, the Fermi energy is at the top of the bandgap. However, surface states pin the Fermi energy within the bandgap in the surface region resulting in band bending. The extent of the band bending is not known experimentally, so it is not possible to directly state the relationship between the bias voltage applied to the sample and the conduction band states. This restriction is not actually a significant problem when comparing simulated and experimental STM images because much of the image contrast is due to topographic effects and, as long

as the empty density of states is integrated over a reasonable energy window, further expanding that window does not significantly change the critical features in the simulated images. Therefore, the DFT-calculated Fermi energy for undoped surface models was used as reference value.

Tests were also conducted to determine whether it was necessary to first run the DFT calculations with the artificial incorporation of an external planar field due to the high voltage, but this did not lead to any perceptible changes in the image simulations for this material system, so this was not applied thereafter. For comparison to constant-height images, it would suffice to sample the artificial local density of unoccupied states over a plane parallel to the surface, at a given distance. However, the experimental micrographs were gathered in constant-current mode. Therefore, if we are to directly compare simulated images to experiment (by, for example, monitoring height corrugation), it is necessary to sample the density over a volume rather than a plane. This was done with 0.2 Å in-plane and 0.3 Å out-of-plane sampling intervals, thus generating a 3D array of densities. Since the STM is not perfectly stable and does not have an infinitesimally small tip, blurring was applied to account for tip size, vibration, and thermal effects. For this, each density voxel was convolved in-plane using a radially symmetric step-function convolution, defined by

$$F(r) = \begin{cases} 1, & r \le R \\ 0, & r > R \end{cases}, \tag{4}$$

where r is the distance from the voxel of interest and R defines an effective tip size; $R = 2$ Å was used in the simulations described in this paper.

After convolution, an isosurface of constant density was generated for specified values corresponding to a constant-current imaging mode. The 3D isosurface was then colored with grayscale brightness scaled with height at each in-plane position. The simulated STM image is ultimately the visualization of the isosurface down the axis perpendicular to the surface plane, with the coloring scheme preserving the out-of-plane information.

D. Bond valence sum analysis

The bond valence sum (BVS) of an ion, defined to be positive for cations and negative for anions, is calculated as

$$\mathrm{BVS} = \pm \sum_i \exp((R_0 - R_i)/b), \tag{5}$$

where R is the bond length, R_0 is an experimentally determined standard bond distance for the particular ion pair in question, and b is an empirical constant, typically 0.37 Å. The BVS is in many ways more meaningful than integer formal valences and while they are extensively used to analyze bonding in bulk systems, it has been recently shown that their applicability extends well to surfaces.[25]

Therefore, bond valence sums were calculated for surface Ti atoms in non-defective nanoline models, following DFT relaxation. The following R_0 values were employed to calculate each bond valence: 1.815 Å for $Ti^{4+}-O^{2-}$ and 1.791 for $Ti^{3+}-O^{2-}$.[26] No R_0 value appears to exist in the literature for $Ti^{2+}-O^{2-}$. The volume of each supercell was expanded isotropically to match the lattice parameter to the experimental a_{SrTiO_3} value of 3.905 Å. The bond valence sums were computed using the KDist software from the Kalvados program suite,[27] allowing each Ti atom to adopt its preferred formal state (3+ or 4+) for the calculation. This was repeated for rocksalt TiO for a reference on the 2+ state, borrowing a structure from the literature.[28]

III. RESULTS

A. The c(4 × 2) reconstruction

As expected, the STM images of c(4 × 2)-reconstructed samples[5] show step heights of approximately 0.4 nm (one $SrTiO_3$ bulk unit cell), implying only one type of surface termination. As shown in Fig. 1(c), the main feature in images with bias voltage of 2.0 V is a round bright spot which is present exactly once per c(4 × 2) cell. Since the atomic-scale structure is known in this case, it is possible to generate a STM image simulation for direct comparison and subsequent attribution of the bright feature to a particular structural element. The 2.0 V DFT-based simulation of the relaxed c(4 × 2) surface is in good agreement with the experimentally observed micrographs, as can be seen in Fig. 1(c); this supports the claim that this structure is the same as the one solved via transmission electron diffraction. Moreover, we can conclusively say that the aforementioned polyhedral quartet motif is responsible for the observed round spot.

B. Dilines

The nanolines form reproducibly on $SrTiO_3$(001) surfaces as shown in the STM image in Fig. 2. One type of nanoline, which appears in the STM images, is the diline. Dilines have a ridge-and-valley structure with 6 × 2 periodicity in close-packed domains. The latter number indicates the periodicity along the [100]-type nanoline growth direction (hereafter "longitudinal" direction) and the former labels the periodicity along its perpendicular (hereafter "transverse") direction. The STM corrugation indicates that the top layer is one atomic layer higher than the known double-layer TiO_2-rich reconstructions such as the aforementioned c(4 × 2), often found as a precursor to (or in coexistence with) nanolines.[4] A characteristic bright round motif is the main building block of the diline structure; it is the stacking of said motifs in two parallel rows that gives the diline its name. This type of nanoline can exist in two configurations: square, where the spots from contiguous rows are aligned along the longitudinal axis; and zigzag, where the spots are "out of phase" by one bulk unit cell with respect to those in the next row. The rows are 0.78 nm apart, so the separation between the centers of adjacent motifs under the square configuration is exactly two bulk unit cells. Auger electron spectra (AES) indicate that dilines are more Ti-rich than cleaved surfaces and double-layer TiO_2-reconstructed structures such as the c(4 × 2).[7]

Numerous candidate nanoline structural models were examined, but only a few are discussed here. Most candidate structures were discarded due to their high surface energy or the poor match to experiment of their simulated STM images.

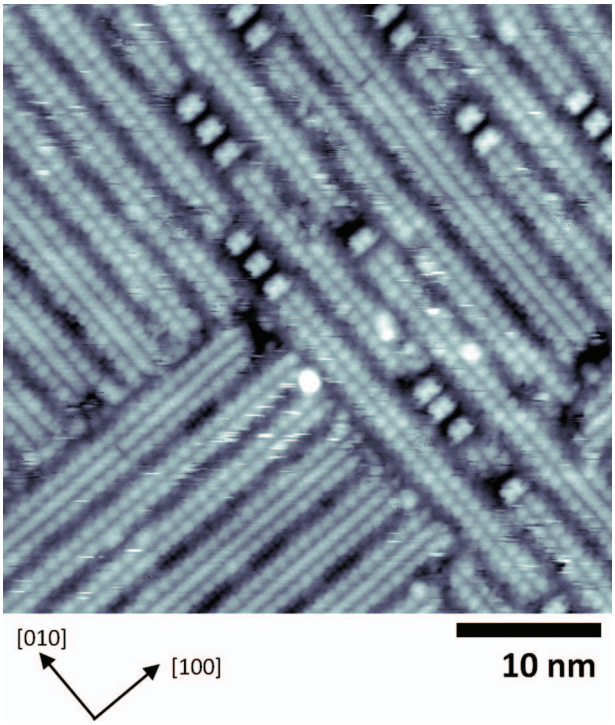

FIG. 2. STM image of a typical nanostructured $SrTiO_3(001)$ surface dominated by dilines and trilines (1.976 V bias, 0.225 nA tunneling current).

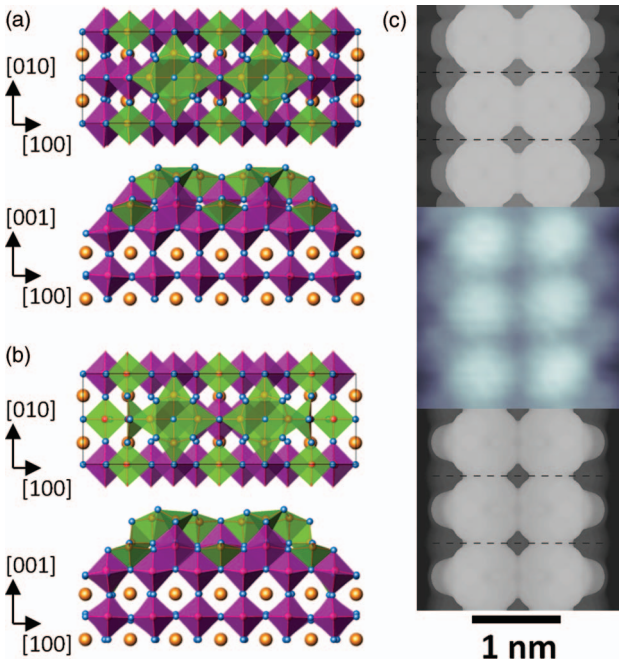

FIG. 3. DFT-relaxed (a) D1, and (b) D2 diline structures, square configuration: plan view (top) and profile view (bottom). STM micrographs, unit cell outlined: D1 simulation (top, 1.5 V bias), experimental (center, 1.7 V bias, 0.05 nA tunneling current), and D2 simulation (bottom, 1.5 V bias).

Based on the observation that these bright spots are of the same size and shape as those in experimental STM images of c(4 × 2) surfaces, diline structural models containing the polyhedral quartet motif on the top layer were created and relaxed in WIEN2k; this is reasonable, as the the c(4 × 2) precedes and coexists with the nanolines. The quartet motif constrains the second layer structure – at least immediately underneath it – upon the assumption of a TiO_x underlayer, consistent with the AES results. Of the two registries with bulk-like TiO_2 layers, the one leading to the central O being in 5-fold coordination is not only significantly lower in energy[10] but is also the observed registry for the c(4 × 2)-reconstructed surfaces. Nonetheless, the structure in the valley area observed via STM must be different.

Two viable models with a perfectly bulk-like TiO_2 third layer were tested, the first one being:

- D1. Qualitatively bulk-like second layer, except for a row of missing TiO along the center of the valley. See Fig. 3(a).

A perfectly bulk-like TiO_2 second layer was not considered, as access to the third layer is necessary to match the valley corrugation measured experimentally. A simulated STM micrograph (1.5 V bias voltage) of the D1 model in the square configuration is shown in the top panel of Fig. 3(c). While this model replicates most diline features, in the experimental micrographs the valley area exhibits distinct semicircular features originating from the second atomic layer, always "out of phase" with the nearby top-layer round motifs, as illustrated in the middle panel of Fig. 3(c). This is not well reproduced by the D1 model, which does show similar such features, but both in phase and out of phase with the top-layer spots, with the former extending further out into the valley. Rather, it appears that in the D1 model the spurious "in-phase" features are due to the 2-fold coordinated O atoms in the second layer, nearest to the center of the valley. Therefore, a modification was made to arrive at a new model:

- D2. Qualitatively the same as D1, except for the removal of only those second-layer oxygen atoms that were in phase with the top-layer features; this keeps all Ti atoms in at least 5-fold coordination.

Figure 3(b) shows the relaxed structure, under the square configuration and the 1.5 V simulated STM image is presented in the bottom panel of Fig. 3(c). This model successfully reproduces the second-layer valley features. Crystallographic information files (CIF) of the relaxed structure, in both square and zigzag configurations, are available in the supplementary material.[29]

C. Trilines

Another type of nanoline is the triline, which is sometimes observed in coexistence with the diline. Trilines are similar in appearance to the dilines, except for the additional presence of a "backbone" between diline-like rows. Trilines have 8 × 2 or 9 × 2 periodicity when found in close-packed domains, with the valley size determining the transverse period. X-ray photoelectron spectra (XPS) show more Ti reduction than in diline spectra, as nominally "2+" Ti 2*p* peaks, absent for diline-covered surfaces, appear.[22] Structural triline models based on the D2 architecture were examined, keeping the valley and diline-like top-layer motifs unchanged, and thus leaving only the backbone structure to be determined.

The backbone building blocks have single-unit-cell periodicity (0.39 nm) along the longitudinal direction.[22] Each of these units has mirror symmetry along both the longitudinal and transverse directions. Within these constraints, three structural models of 8×2 periodicity were initially constructed, relaxed, and employed for STM image simulations:

- T1. A segment of a bulk-like TiO_2 plane makes up the top layer of the backbone, via two rows of corner-sharing TiO_5 polyhedra running along the longitudinal direction. The O* atoms (labeled in Fig. 4(a)) are shared with the diline-like quartet motif when the nearby backbone Ti is in phase with it. Each backbone top-layer unit is thus Ti_2O_5 in this case.
- T2. Similar to the T1, but with an additional Ti atom in the otherwise hollow sites along the central column of the backbone; this leads to a Ti/O checkerboard pattern along the backbone top layer (see Fig. 4(b)). The extra Ti atoms are thus also 5-fold coordinated and this leads (as in the quartet motif) to not just corner-sharing, but edge-sharing TiO_5 polyhedra. In this model, the top-layer repeat units are Ti_3O_5. This composition indicates some reduction, consistent with the XPS data; this shall be quantified in Subsection III D.
- T3. Similar to T1, but with additional Ti in the octahedral sites of the backbone second layer (four per triline supercell), thereby creating a local Ti/O checkerboard pattern under the backbone top layer. The top layer is still Ti_2O_5, but the reduction in the underlayer is also consistent with the XPS results. Its polyhedral representation in the square configuration and its corresponding 1.5 V STM image simulation are available in the supplementary material.[29]

The 1.5 V simulation for model T1 shows a less bright (less height, i.e., the density isosurface is closer to the sample) backbone signal than for the adjacent diline-like features (Fig. 4(c)). Furthermore, within every backbone repeat unit each Ti appears as its own distinct spot, instead of pairing up and combining as a single unit. Moreover, some of the quartet O atoms brighten up markedly more than the rest.

Model T2 gives the best match to experiment, with the backbone and diline-like features having comparable intensities and the backbone repeat units appearing each as a single feature. One such simulation, in the zigzag configuration, is shown in Fig. 4(c); a CIF of this structural model is available in the supplementary material.[29]

The corresponding simulations for model T3 present the same problem as T1, in that the top-layer backbone Ti atoms give rise to resolved small spots. Moreover, the brightness from in-phase backbone units appears to extend into part of the adjacent (and otherwise less bright) diline-like motif.

It must be mentioned that the triline backbone defect (see below) does not significantly depend on the neighboring diline-like features. That is, its existence is equally frequent under the zigzag and square configurations, and within the latter it is equally common in the in-phase and out-of-phase locations; this also holds true for its diffusion rate. This seems to suggest that the triline backbone ought to be independent

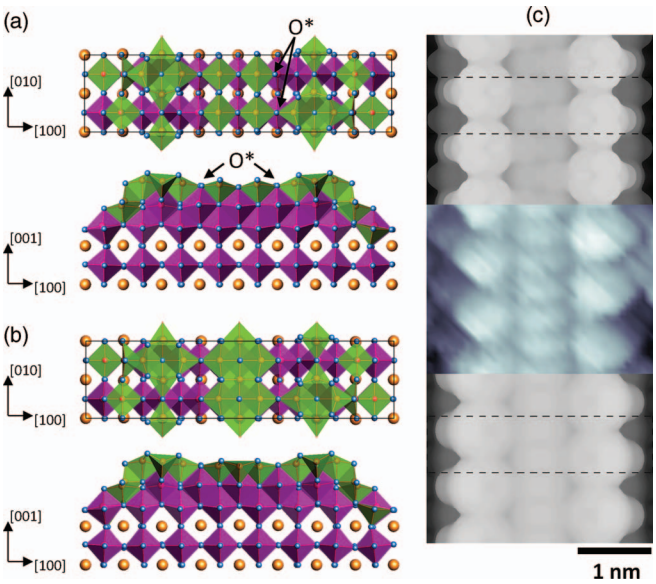

FIG. 4. (a) T1, and (b) T2 triline structures in the zigzag configuration: plan view (top) and profile view (bottom). (c) STM micrographs, unit cell outlined: T1 simulation (top, 1.5 V bias), experimental (middle, 2.23 V bias, 0.24 nA tunneling current), and T2 simulation (bottom, 1.5 V bias).

of the diline-like motifs, so another structural model was generated and tested:

- T4. Similar to T2, it keeps the additional top-layer Ti atoms in the backbone. However, the O* atoms originally bonded to the outside of the backbone Ti (half of which bridge the backbone to the diline-like features) are no longer present. The second atomic layer remains bulk-like underneath the backbone. The polyhedral representation of the T4 model in the zigzag configuration and its corresponding 1.5 V STM image simulation are available in the supplementary material.[29]

The simulated micrograph of the T4 model clearly fails to reproduce the experimental backbone features; the removal of the mentioned O leads to high brightness where the Ti–O bond existed, spuriously dominating the backbone signal.

For completeness, we note that other structures not discussed here came close to matching the experimental STM images but were not consistent with the backbone defect discussed in Subsection III E. Model T2 provides the best fit both in itself, as well as with the constraints imposed by the backbone defect.

D. Surface Ti valence states

Since the chemical shifts of XPS peaks actually reflect changes in bond valence sums (and not the idealized integer valence states), one can attempt to explain the appearance in trilines (and absence in dilines) of "Ti^{2+}" peak shoulders via BVS analysis. For this purpose, BVS values of the top-layer Ti atoms were computed for the favored D2 and T2 models. The results are listed in Table I, and the atom labels refer to the respective CIF files. For further clarity, the Ti4, Ti6, and Ti7 atoms correspond to the Ti sites in the $c(4 \times 2)$-like quartet motifs. Within the T2 structure, the rest are Ti sites

TABLE I. Bond valence sums for Ti atoms in the D2 and T2 nanoline models, and in rocksalt TiO. Atom labels refer to the CIF files.

D2 diline		T2 triline		Rocksalt TiO (Ref. 28)	
Atom	BVS	Atom	BVS	Atom	BVS
Ti4	3.84	Ti4	4.00		
Ti6	4.13	Ti6	4.15		
Ti7	3.97	Ti7	3.97		
		Ti11	3.72		
		Ti12	2.87	Ti	2.69
		Ti13	3.65		

in the backbone. The Ti11 site is along the center row in the backbone, at the center of the TiO_5 polyhedron sharing its edges with four other polyhedra. Each Ti12 atom is in phase with the quartet motif, sharing an O with it. Finally, each Ti13 atom is out of phase with the nearby polyhedral quartets.

The Ti atoms within the polyhedral quartets in either structure have bonding that is very close to a formal 4+ state. However, the Ti in the triline backbone are reduced, especially the Ti12 atom, since the O atoms it is bound to are heavily constrained. As a reference for the BVS of a Ti^{2+} state when calculated using the Ti^{3+}–O^{2-} R_0, Ti atoms in rocksalt TiO have a bond valence sum of 2.69, close to the Ti12 value. The appearance of low-binding-energy shoulders in the XPS data[22] is easily explained by the T2 model.

E. Backbone defect

A characteristic triline defect appears in experimental STM micrographs. It shows up essentially as a missing repeat unit within the backbone,[22] so it is double mirror-symmetric itself and is always in phase or out of phase with the diline-like features. Thus, the T2 model rules out the possibility that the defect is a single Ti vacancy, since the center of the diline-like spots always line up with a pair of Ti atoms, never just one. Moreover, the STM image of a single Ti vacancy was simulated in small supercell calculations and indeed, it results in a small dark feature between repeat units, which is further reason to discard this option. All triline models indicate that most of the triline backbone brightness in experimental micrographs is due to pairs of top-layer Ti atoms. This in turn eliminates the possibility of it being a single O vacancy.

An analysis of defect position along the backbone as a function of time allowed for the extraction of its hopping rate. In turn, this was fitted to an Arrhenius diffusion equation, as explained in Ref. 22, which yields a defect diffusion activation energy of 4.98 ± 0.17 eV; the large value supports the conclusion that the defect cannot consist of a single atom, and must be more complex.

In order to test defect models more efficiently, 4 × 4 supercells (the valleys were excluded) with 7 atomic layers were generated; see Fig. 5 for clarity. This forcibly required the use of the square configuration. Defects aligned with the diline-like motifs were initially modeled. To begin with, two structural models were constructed for the backbone defect:

- BD1. A pair of Ti vacancies aligned "in phase" with the diline-like features, and the outside O*-type also missing (two Ti-O pairs removed). Its polyhedral representation and STM image simulation are available in the supplementary material.[29]
- BD2. A vacant linear Ti_2O_3 unit. That is, the same as BD1, but with the central O between the Ti atoms also removed. Its polyhedral representation and corresponding simulated STM micrograph are available in the supplementary material.[29]

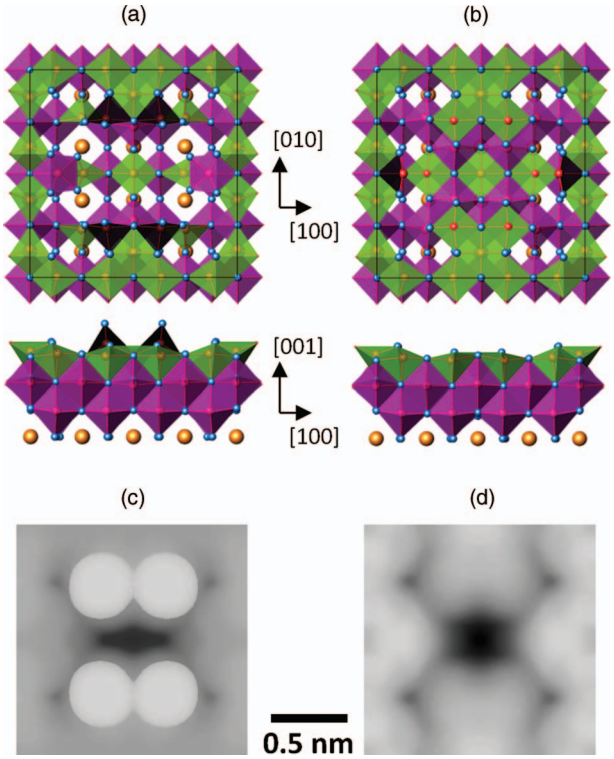

FIG. 5. Simplified 4 × 4-supercell models of (a) BD3 and (b) BD4 models of triline backbone defect in phase with diline-like features, square configuration. Plan view (top) and profile view (bottom). 1.5 V simulated STM micrographs: (c) BD3, and (d) BD4.

Both BD1 and BD2 prove inadequate. The STM image simulations show an enhanced signal from the nearby O atoms, as a result of their out-of-plane relaxation. Also, the simulated image for the BD1 model shows necking between the features on either side of the defect; the bridging O is responsible for this, as it has nonzero local density of unoccupied states. Meanwhile, while a gap exists in the defect of the BD2 simulation, it is too narrow, not the size of a repeat unit. Therefore, a third structural model was studied:

- BD3. Similar to the BD2 defect model, but with the two nearby central-row Ti atoms also vacant, thereby constituting a larger Ti_4O_3 vacancy cluster; see Fig. 5(a).

Upon relaxation, the four O atoms nearest to the defect core (each only bound to one Ti atom) lift up much more, resulting in rather vertical titanyl bonds. These overwhelmingly dominate the STM image simulations. However, an adequately sized gap emerges in the defect core. In order to address the remaining discrepancy, a fourth model was created:

- BD4. The same Ti_4O_3 cluster as in model BD3 was removed, but each of the 4 (previously removed) Ti atoms are instead placed in one of the empty octahedral sites in the layer underneath. This keeps the top-layer O from lifting up as they do in model BD3. In this arrangement, only three O atoms are effectively missing.

The simulated STM image is a good fit to experiment, showing a dark, oval-shaped defect region – essentially a missing repeat unit (see Fig. 5(b)). The backbone exhibits a unit of brighter signal half way in between contiguous defects, but we believe this is an artifact of the small periodicity imposed.

One similar model was investigated:

- BD5a. This is qualitatively the same as model BD4, except for the no-longer removed O atoms which bridge (in the non-defective structure) the backbone with the diline-like features. In this scenario, only one O atom is effectively missing. The polyhedral representation of this structure and its 1.5 V STM image simulation are available in the supplementary material.[29]

The simulation of the STM micrograph successfully reproduces the dark defect and is more elliptical than in the BD4 simulation. Nonetheless, there is plenty of undesired brightness contrast – namely, the backbone units, which are immediately adjacent to the defect, are more prominent than the rest. Similarly, the diline-like features, which are aligned with the defect, are much brighter than those near the non-defective backbone segment. While the brightness disparity is larger and less local than that found for BD4, in principle this may be due to the artificially imposed small periodicity. In order to indirectly test the BD5a model, another model with the same stoichiometry was examined. It must be emphasized, however, that the following structure was not itself a candidate for the defect structure, as it did not satisfy several of the known constraints.

- BD5b. A linear Ti–O–Ti unit running along the central row of the backbone top layer is removed. Two Ti atoms are placed in two of the four nearby empty octahedral sites in the second layer. These two atoms occupy opposite sites with respect to the center of the defect, thereby breaking the mirror planes but preserving the 2-fold rotational symmetry. The polyhedral representation of this structure is available in the supplementary material.[29]

This defect structure is calculated to be 1.3 eV lower in energy than model BD5a. Therefore, BD5a is not stable, since two of its subsurface Ti would quickly migrate back to the top layer. Moreover, should the BD5a defect occur at a backbone position out of phase with the diline-like features (square configuration), this would leave two highly unstable O atoms, bound only to one Ti; half as much is true at every position along the backbone under the zigzag configuration. Including these O atoms as part of the vacancy cluster is of course unviable, as the number of these varies depending on the defect position (1 in square in-phase, 2 in zigzag, 3 in square out-of-phase). As mentioned above, the diffusion dynamics show no discernible dependence on defect position. This in itself suffices to discard all structural models (for example, just two Ti vacancies), which do not include the side O in the vacancy cluster.

Model BD4 was thereafter simulated in the out-of-phase square configuration. While not identical to the in-phase case, the simulated image of this configuration (available in the supplementary material[29]) also succeeds in reproducing the defect as a missing backbone unit. Ultimately, this defect structure was also modeled with a larger (8×4) supercell, which includes the valley areas, as well as four additional atomic layers in the bulk, for a total of 890 atoms. A composite figure of the STM simulation of the defect under the zigzag configuration and the perfect triline is shown in Fig. 6, along with a typical experimental image. A CIF of this structure is available in the supplementary material.[29]

IV. DISCUSSION

It is clear that the polyhedral quartet motif which characterizes the $c(4 \times 2)$ reconstruction is a recurrent feature of many stable $SrTiO_3(001)$ surfaces. It is the main building block in titanium-rich dilines, which in turn are the cornerstone for the formation of the trilines. Moreover, while this motif is likely to play a role in the stabilization of the surfaces of other perovskite (ABO_3) materials, this is constrained to BO_2-rich surfaces. The planar registry of the polyhedral quartet with a rocksalt-like AO plane is energetically unfeasible in such structures.

The non-defective structural solutions of the nanolines satisfactorily consist of Ti-centered polyhedra at the surface, where all top-layer Ti are fivefold coordinated and every polyhedron is in an edge-sharing configuration with at least two other such polyhedra. In general, the edge-sharing arrangement of surface polyhedra prevents many surface O from being in single co-ordination, given the registry of the top layer with the bulk-like layer below.

In particular, the dilines borrow the characteristic quartet motif but with an extra Ti-rich layer. The second layer is not fully bulk-like but supports the quartet motifs and provides a valley area that successfully reproduces the experimental STM images. Moreover, it is worth noting that the zigzag and square configurations take up slightly different amounts of oxygen.

The triline builds on the diline structure, but adds a backbone with a top-layer checkerboard pattern of Ti and O, with a more Ti-rich composition than the dilines. The nanolines can adapt to small variations in Ti and O content by adopting different structures, while maintaining the quartet motif. Admittedly, we cannot be absolutely definitive about the exact composition under the outermost atoms, but the triple-layer TiO_x models proposed here are consistent with the AES data. Moreover, BVS analysis of these structures predicts the presence of reduced Ti sites only in triline-covered surfaces, in accordance to XPS results. A detailed report of the XPS data is presented in Ref. 30 along with a discussion of the

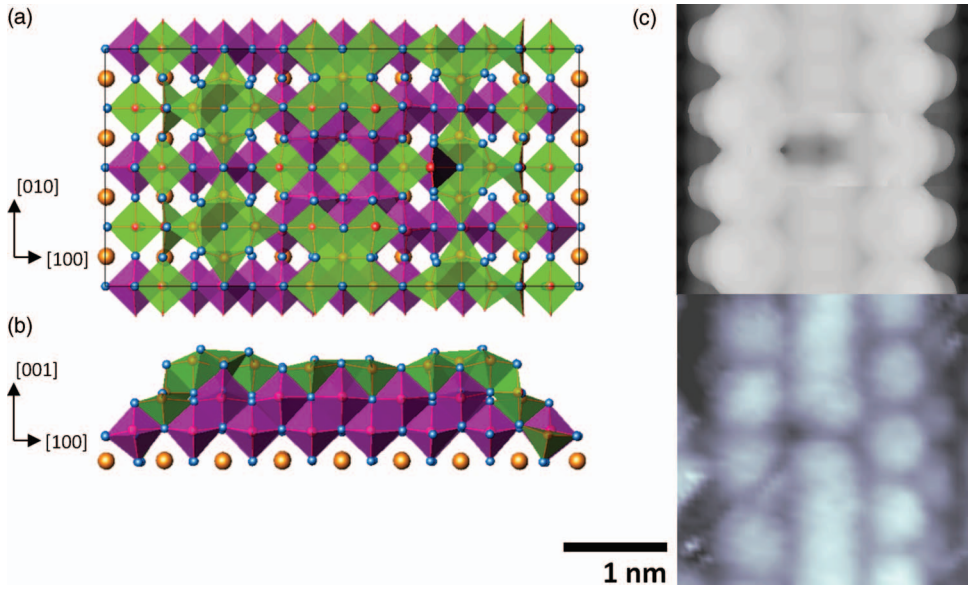

FIG. 6. Relaxed 8 × 4-supercell structural model of BD4 triline backbone defect in the zigzag configuration: (a) plan view, with cell outlined, and, (b) profile view. (c) Composite image of 1.5 V simulated STM micrographs of T2 triline model and BD4 zigzag model (top), and experimental STM image of backbone defect in the zigzag configuration (bottom, 2.25 V bias, 0.24 nA tunneling current).

electronic structure of the diline and triline models, showing the generation of mid-bandgap surface states.

The triline backbone defect is large and complicated, consisting of three effective oxygen vacancies plus four relocated Ti atoms in new subsurface positions. This complexity is required by symmetry constraints, as well as by the electronic structure and observed hopping rate. No single vacancy defect can reproduce the experimentally observed defect hopping, and the diffusion activation energy of 4.98 ± 0.17 eV is too large for a single-atom defect structure; for comparison, the barrier for single O vacancy diffusion in bulk $SrTiO_3$ is calculated to be in the 0.40–0.58 eV range[31,32] and the corresponding value for diffusion along a TiO_2-terminated (001) surface is ∼0.11 eV.[32] The dynamics of defect motion along the length of the triline backbone, as illustrated in Fig. 7, require a collective effort. For a translation of one bulk unit cell to occur, three subsurface Ti atoms must hop to top-layer sites and three top-layer Ti must hop to octahedral second-layer sites. Additionally, three surface O atoms must jump to new positions. Unfortunately, vast computational expense keeps us from estimating the activation energy of such an orchestrated motion, but we believe this diffusion scheme explains the large observed activation barrier.

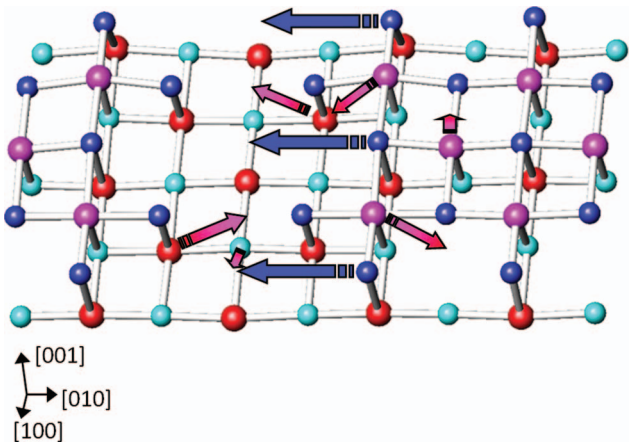

FIG. 7. Schematic ball-and-stick representation of the diffusion mechanism of the BD4 defect along triline backbone. Topmost two layers of 2 × 4 triline backbone supercell are shown, and structure shown is not relaxed. Longitudinal direction is [010] and transverse is [100]. Surface Ti are pink, subsurface Ti are red, surface O are blue, and subsurface O are light blue.

V. CONCLUSION

We have shown that the first-principles simulation of scanning tunneling micrographs is a powerful tool for surface structure determination efforts, even for insulating materials which require doping and high experimental bias voltages. Structural models have been put forward for the dilines, trilines, and triline backbone defect, all consistent with the observed scanning tunneling micrographs and complementary spectroscopic data. In particular, the Ti-rich nanolines on $SrTiO_3$(001) surfaces are terminated by three TiO_x layers and exploit the polyhedral quartet feature which is characteristic of the c(4 × 2) reconstruction. In this way, we demonstrate that the polyhedral quartet motif found in multiple surfaces is a fundamental unit of reconstructed $SrTiO_3$(001) surfaces.

ACKNOWLEDGMENTS

This research was supported by the National Science Foundation under Grant No. DMR-0906306.

[1]J. G. Mavroides, J. A. Kafalas, and D. F. Kolesar, Appl. Phys. Lett. **28**, 241 (1976).
[2]P. Chaudhari, R. Koch, R. Laibowitz, T. McGuire, and R. Gambino, Phys. Rev. Lett. **58**, 2684 (1987).
[3]A. Ohtomo and H. Y. Hwang, Nature (London) **427**, 423 (2004).
[4]M. R. Castell, Surf. Sci. **516**, 33 (2002).
[5]M. R. Castell, Surf. Sci. **505**, 1 (2002).
[6]F. Silly and M. R. Castell, J. Phys. Chem. B **109**, 12316 (2005).
[7]D. S. Deak, F. Silly, D. T. Newell, and M. R. Castell, J. Phys. Chem. B **110**, 9246 (2006).

[8]N. Erdman, K. R. Poeppelmeier, M. Asta, O. Warschkow, D. R. Ellis, and L. D. Marks, Nature (London) **419**, 55 (2002).
[9]N. Erdman, O. Warschkow, M. Asta, K. R. Poeppelmeier, D. R. Ellis, and L. D. Marks, J. Am. Chem. Soc. **125**, 10050 (2003).
[10]O. Warschkow, M. Asta, N. Erdman, K. R. Poeppelmeier, D. E. Ellis, and L. D. Marks, Surf. Sci. **573**, 446 (2004).
[11]C. H. Lanier, A. Van de Walle, N. Erdman, E. Landree, O. Warschkow, A. Kazimirov, K. R. Poeppelmeier, J. Zegenhagen, M. Asta, and L. D. Marks, Phys. Rev. B **76**, 045421 (2007).
[12]M. Kawasaki, A. Ohtomo, T. Arakane, K. Takahashi, M. Yoshimoto, and H. Koinuma, Appl. Surf. Sci. **107**, 102 (1996).
[13]R. Herger, P. R. Willmott, O. Bunk, C. M. Schlepütz, and B. D. Patterson, Phys. Rev. Lett. **98**, 076102 (2007).
[14]E. Heifets, S. Piskunov, E. A. Kotomin, Y. F. Zhukovskii, and D. E. Ellis, Phys. Rev. B **75**, 115417 (2007).
[15]D. M. Kienzle, A. E. Becerra-Toledo, and L. D. Marks, Phys. Rev. Lett. **106**, 176102 (2011).
[16]D. S. Deak, F. Silly, K. Porfyrakis, and M. R. Castell, J. Am. Chem. Soc. **128**, 13976 (2006).
[17]D. S. Deak, F. Silly, K. Porfyrakis, and M. R. Castell, Nanotechnology **18**, 075301 (2007).
[18]P. Blaha, K. Schwarz, G. K. H. Madsen, D. Kvasnicka, and J. Luitz, *WIEN2k, An Augmented Plane Wave + Local Orbitals Program for Calculating Crystal Properties* (Universität Wien, Vienna, 2010).
[19]J. P. Perdew, K. Burke, and M. Ernzerhof, Phys. Rev. Lett. **77**, 3865 (1996).
[20]J. Tersoff, and D. R. Hamann, Phys. Rev. Lett. **50**, 1998 (1983).
[21]J. Bardeen, Phys. Rev. Lett. **6**, 57 (1961).
[22]M. S. J. Marshall, A. E. Becerra-Toledo, L. D. Marks, and M. R. Castell, Phys. Rev. Lett. **107**, 086102 (2011).
[23]K. Stokbro, U. Quaade, and F. Grey, Appl. Phys. A **66**, S907 (1998).
[24]C. J. Chen, *Introduction to Scanning Tunneling Microscopy* (Oxford University Press, New York, 1993).
[25]J. A. Enterkin, A. E. Becerra-Toledo, K. R. Poeppelmeier, and L. D. Marks, Surf. Sci. **606**, 344 (2012).
[26]I. D. Brown and D. Altermatt, Acta Crystallogr., Sect. B: Struct. Commun. **41**, 244 (1985).
[27]K. Knížek, Kalvados – Software for crystal structure and powder diffraction; see http://www.fzu.cz/~knizek/kalvados/index.html.
[28]R. W. G. Wyckoff, *Crystal Structures*, Vol. 1 (Interscience Publishers, New York, 1963).
[29]See supplementary material at http://dx.doi.org/10.1063/1.4719212 for structural models and STM simulations not imaged in the main article, as well as for relevant CIF files.
[30]M. S. J. Marshall, A. E. Becerra-Toledo, D. J. Payne, R. G. Egdell, L. D. Marks, and M. R. Castell, "Structure and composition of linear TiO_x nanostructures on $SrTiO_3$(001) surfaces" (unpublished).
[31]M. Lontsi-Fomena, A. Villesuzanne, J. P. Doumerc, C. Frayret, and M. Pouchard, Comput. Mater. Sci. **44**, 53 (2008).
[32]J. Carrasco, F. Illas, N. Lopez, E. A. Kotomin, Y. F. Zhukovskii, R. A. Evarestov, Y. A. Mastrikov, S. Piskunov, and J. Maier, Phys. Rev. B **73**, 064106 (2006).